analytical chemistry

Technical Note

pubs.acs.org/ac

Three-Dimensional Elemental Imaging of Nantan Meteorite via Femtosecond Laser Ionization Time-of-Flight Mass Spectrometry

Miaohong He,[†] Yifan Meng,[†] Shanshan Yan,[†] Wei Hang,*[,†,‡] Wenge Zhou,[§] and Benli Huang[†]

[†]Department of Chemistry and the MOE Key Lab of Spectrochemical Analysis and Instrumentation, College of Chemistry and Chemical Engineering, Xiamen University, Xiamen, Fujian 361005, China

[‡]State Key Laboratory of Marine Environmental Science, Xiamen University, Xiamen, Fujian 361005, China

[§]Key Laboratory for High Temperature and High Pressure Study of the Earth's Interior, Institute of Geochemistry, Chinese Academy of Sciences, Guiyang, Guizhou 550081, China

ABSTRACT: Femtosecond laser ionization time-of-flight mass spectrometry (fs-LI-TOFMS) is introduced for the three-dimensional elemental analysis of a Nantan meteorite. Spatially resolved multielemental imaging of major and minor compositions in a meteorite are presented with a lateral resolution of 50 μm and a depth resolution of 7 μm. Distinct 3D distributions of siderophile, lithophile, and chalcophile elements are revealed. Co and Ni are highly siderophile (Iron-loving), mainly enriched in the metal phase. Cr, Cu, V, and Mn are enriched in the sulfide for their chalcophile (S-loving) tendency. S, P, and C aggregate together in the analytical volume. Silicate inclusion, containing lithophile elements of Al, Ca, Mg, K, and so on, is embedded within the metal phase for the immiscibility between silicate inclusion and the melted metal phase. These 3D distributions of elements aid the exploration of the formation and evolution of the meteorite. They also reveal the feasibility of fs-LI-TOFMS as a versatile tool for 3D imaging.

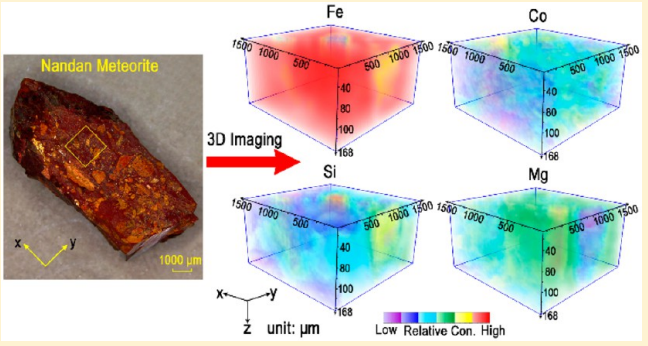

Meteorites, as extraterrestrial materials, carry valuable primitive information about the origin, formation, and evolution of the early solar system. Therefore, studying meteorites is of fundamental importance for tracing the history of the solar system as well as gaining understanding of our own planet Earth.[1] The total composition of a meteorite can basically be acquired by various techniques.[2,3] Nevertheless, a meteorite would undergo a mineral-dependent condensation process during formation followed by fractional crystallization or crystal-segregation,[4−6] which results in inhomogeneous compositions. Thus, elemental imaging should be regarded as a proper method to reveal information about meteorites.

Traditional elemental imaging techniques primarily address the distribution of the surface composition.[7] However, the inner composition of meteorites, which cannot be viewed via naked eyes, is different from the surface. On one hand, the meteorite was formed in a reducing atmosphere. When it passed through the Earth's atmosphere, its surface was exposed to an oxidizing condition. Intense friction as well as impact with the atmosphere resulted in the occurrence of melting on its surface, during which its surface composition would undergo oxidation and volatilization.[2] On the other hand, generally, meteorite surfaces had long been subjected to weathering in the Earth's physical−chemical environment before they were found and collected.[1,8] All of these could make the surface composition different from that of the inner bulk. Therefore, for acquiring complete and accurate information about the formation and evolution of a meteorite, the performance of 3D elemental imaging on meteorites is particularly imperative.

At present, 3D elemental imaging is primarily achieved by either optical spectrometry or mass spectrometry. Optical spectrometry 3D elemental imaging techniques (such as neutron resonance transmission (NRTI),[9] X-ray fluorescence (XRF),[10,11] confocal μ-X-ray absorption near edge structure (μXANES),[12] laser-induced breakdown spectroscopy (LIBS),[13,14] etc.) are simple, straightforward, and microdestructive, yet they usually suffer from spectral interferences and limited detectable elements.[15,16] Mass spectrometry 3D elemental imaging is typically based on the ablation or sputtering of the target via a laser or an ion beam. It is able to construct a 3D map of the spatial compositions within the target.[17] The leading 3D elemental imaging mass spectrometry methods are secondary ion mass spectrometry (SIMS)[18] and laser ablation inductively coupled plasma mass spectrometry (LA-ICPMS).[19−22] General LA-ICPMS is capable of imaging analysis of solids;[22,23] the extreme difficulty of obtaining imaging-related standards for quantitative calibration limits its further application. While SIMS has excellent lateral resolution as well as depth resolution, it is defective in its quantitative capability and the rigorous requirements for the morphology of a sample.

Received: September 8, 2016
Accepted: December 1, 2016
Published: December 1, 2016

DOI: 10.1021/acs.analchem.6b03540
Anal. Chem. 2017, 89, 565−570

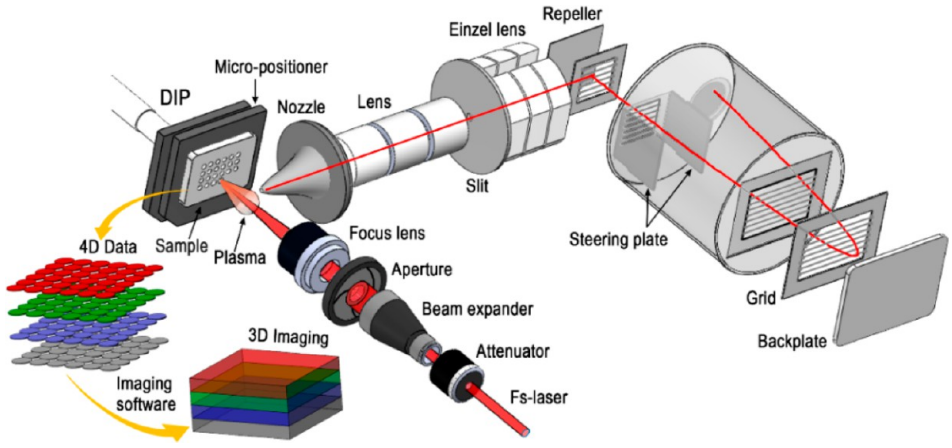

Figure 1. Schematic diagram of the fs-LI-TOFMS system.

Buffer-gas assisted high-irradiance femtosecond laser ionization time-of-flight mass spectrometry (fs-LI-TOFMS) is another mass spectrometry technique based on laser ablation and the ionization method. Unlike the present laser related mass spectrometry 3D elemental imaging techniques, the femtosecond laser was introduced instead of a nanosecond laser because of its suppressed thermal effects during laser−material interaction,[24−27] which offers fs-LI-TOFMS a more uniform ablation and minimized matrix effect.[25] It is capable of directly semiquantitatively determining almost all elements simultaneously without standards.[28] The buffer-gas was brought into the source for diminishing the interference of multiply charged ions via collision and three-body recombination.[29] Furthermore, some pioneering experiments have proved its capability for depth profiling as well as surface elemental imaging,[24,30,31] which has also been proved by other groups using a similar technique.[32,33] Therefore, it allows visualization of the lateral distribution and the depth profile of an element in the material simultaneously. Consequently, fs-LI-TOFMS has the potential for 3D elemental imaging. In this study, a self-prepared disc, which mixes four high purity metal powders of Cr, Fe, Ni, and Cu, is first introduced to exhibit its feasibility. Then, the Nantan meteorite is analyzed to reveal its capability for 3D spatial imaging of an actual heterogeneous sample.

EXPERIMENTAL SECTION

Sample Preparation. Four stoichiometric amounts of 80-mesh metal powders (99.99%) of Cr, Fe, Ni, and Cu were mixed manually and, then, loaded into a die and pressed into a disc and polished prior to analysis. The other sample is a Nantan iron meteorite, which was provided by the Institute of Geochemistry, Chinese Academy of Science. The falling time of the meteorite to the Earth could date back to the year of 1516, and before that, it had wandered among interplanetary space for billions of years.[34] The primary falling areas were located around Nantan county, Guangxi province, China. Therefore, it was named after the county. It is regarded as the second largest iron meteorite in China. Nineteen specimens weighing approximately 9.5 tons have been found up to now.[34] To accommodate the room limitation of the sampling source, a bulk with a relatively flat surface (Figure 5a) was sliced with a diamond wafering blade cutter and cleaned with ethanol solution in an ultrasonic bath.

Instrumental and Analytical Procedures. The study was carried out on a buffer-gas assisted high irradiance femtosecond laser ionization time-of-flight mass spectrometry (fs-LI-TOFMS) system, which is shown in Figure 1. It has been described previously with a few modifications.[25,30] Briefly, the femtosecond laser (S-pulse HP, Amplitude Systemes, France) with a duration of 500 fs, a wavelength of 1030 nm, a frequency of 10 Hz, and an irradiance of 8×10^{13} W/cm^2 was employed. A set of optical components, which include a continuously variable beam attenuator (ABSO-6.35, CVI Melles Griot, USA), a 4× beam expander (Laserlands Laser Equipment, China), and an aperture (iris) (Winner Optical Instrument, China) with an optimized diameter of 4 mm, were used to shape the laser beam into a quasi top-hat profile. Ultrahigh purity helium (99.999%) acting as the buffer-gas was introduced into the ion source of 600 Pa. A series of ionic optical lenses adjoining the nozzle were used as a transportation stage for focusing and guiding the ion beam. The orthogonal "pulse train" repelling mode was employed in the TOFMS with angular reflection.[28]

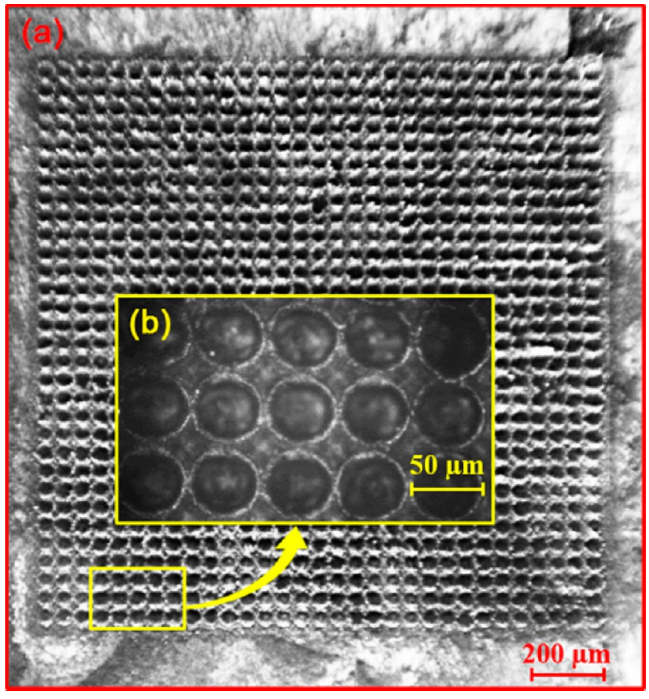

Figure 2. (a) Photograph of 30 × 30 crater array of the self-prepared disc with 35 laser shots for each crater; (b) magnified section.

DOI: 10.1021/acs.analchem.6b03540
Anal. Chem. 2017, 89, 565−570

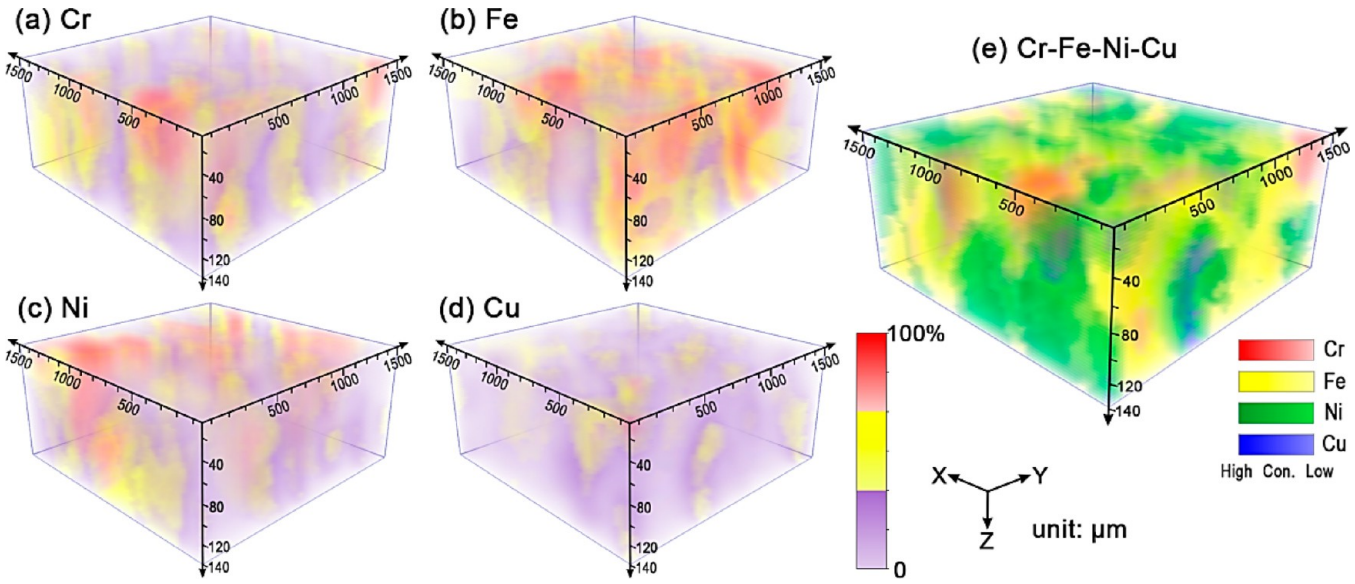

Figure 3. 3D elemental distribution for (a) Cr, (b) Fe, (c) Ni, and (d) Cu on the self-prepared disc; (e) distribution of 4 kinds of metal particles in the ablated cuboid section.

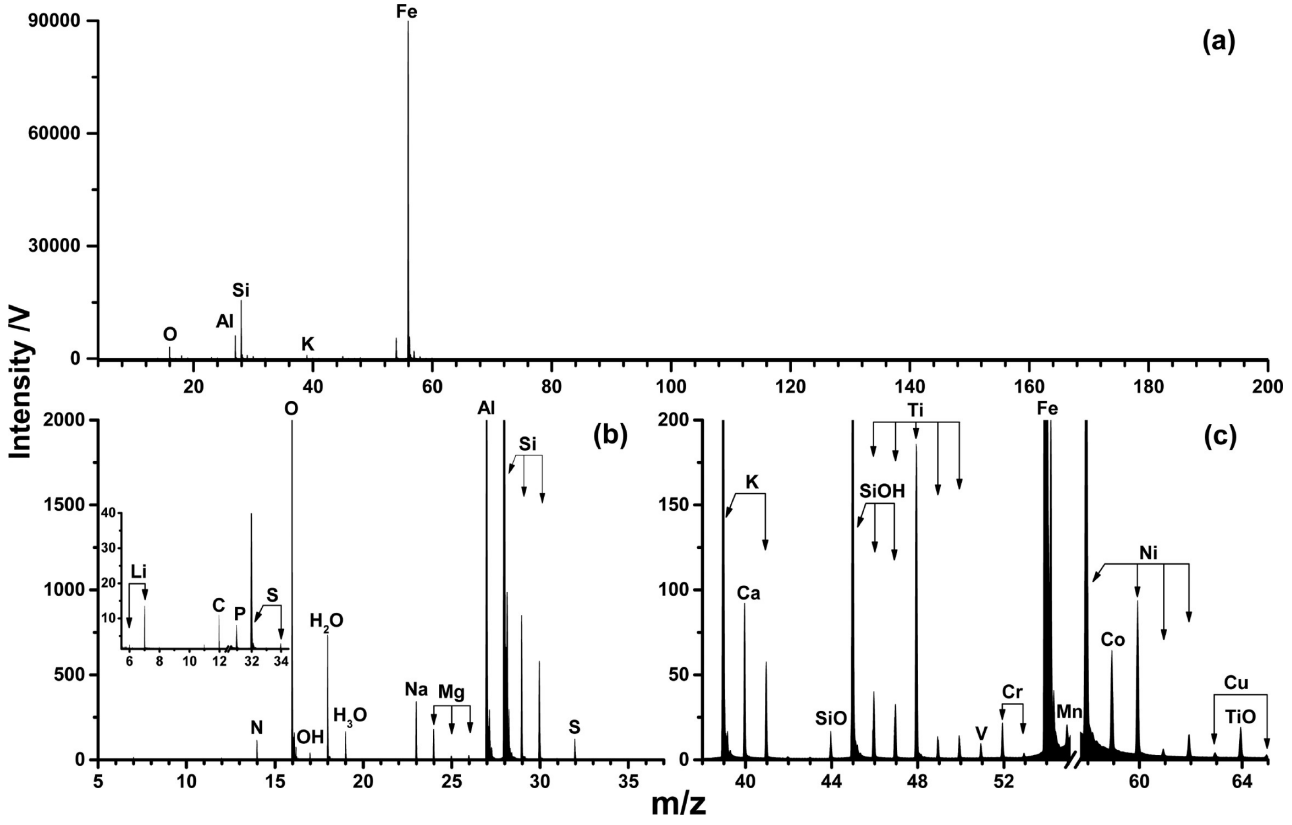

Figure 4. Accumulated spectrum of the entire imaging area. (a) Overview of the spectrum. Magnified portions at (b) 5−37 and (c) 38−65 amu.

The sample was positioned on an *XY* stage micropositioner (SmarAct GmbH, Oldenburg, Germany). The array for imaging was 30 × 30 spots with a 50 μm interval, which is almost equal to the diameter of the laser focusing spot. Each ablation spot on the self-prepared disc and the Nantan meteorite went through a sequence of 200 and 240 shots, respectively. For accurately quantifying the results, every 10 mass spectra of the corresponding single laser shots were accumulated and regarded as the chemical information on one spot of an individual layer. Therefore, 3D maps for the self-prepared disc and the meteorite consist of 20 layers and 24 layers, respectively. The ablation depth per pulse was almost constant over a large depth range.[35] Thus, the average depth resolution was approximately 7.0 μm between consecutive layers because the ablation rate was approximately 0.7 μm per pulse. The data were processed by a self-developed LabVIEW program, and finally, 3D elemental images were constructed on the basis of the 4D data (including the three spatial positioning coordinates and the elemental concentration) by Voxler software.

DOI: 10.1021/acs.analchem.6b03540
Anal. Chem. 2017, 89, 565−570

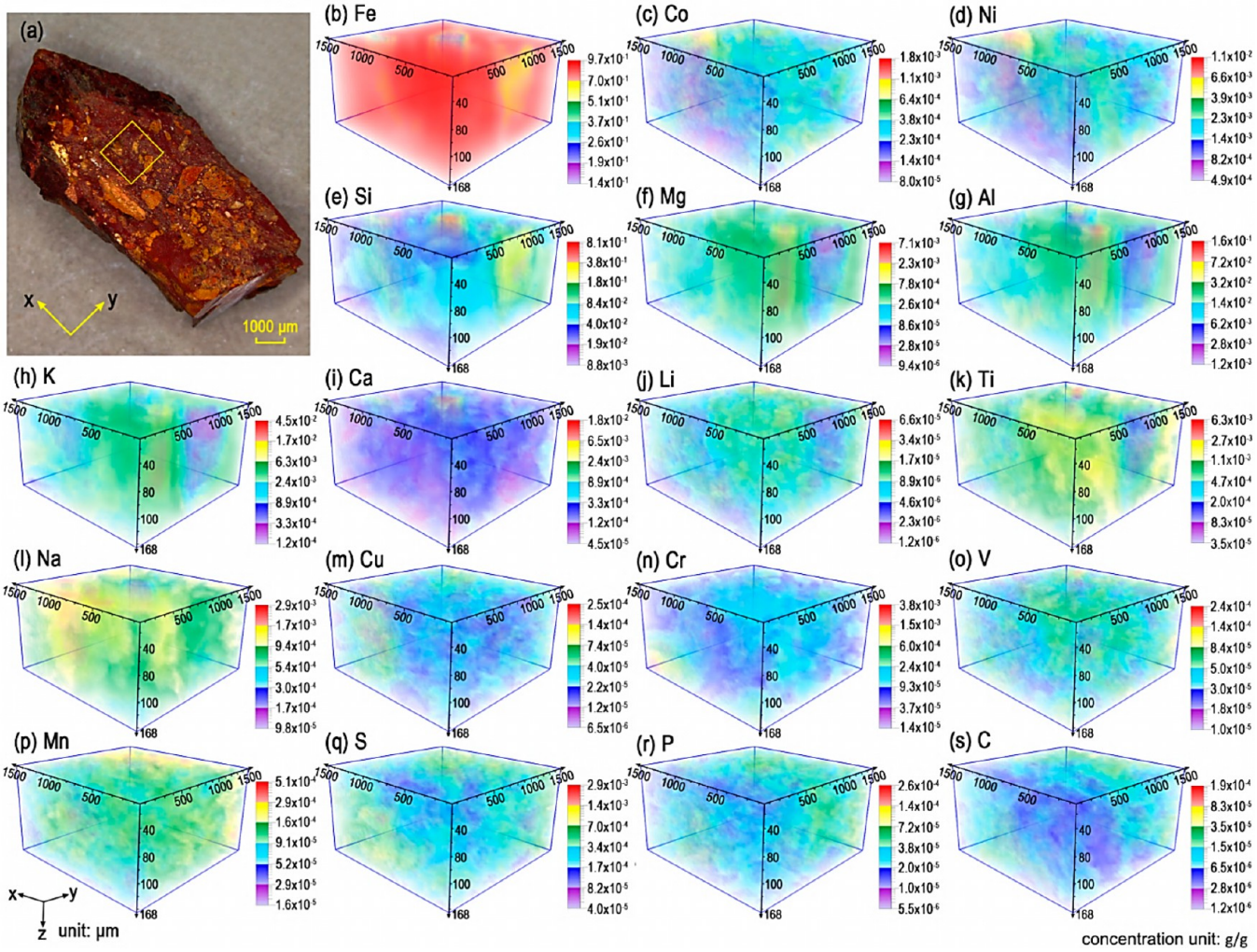

Figure 5. 3D element distributions recorded in the Nantan meteorite. The dimensions of the area are 1.5 × 1.5 mm^2. (a) Photograph of the meteorite and (b–s) particular elemental distributions in the meteorite (g/g in concentration).

RESULTS AND DISCUSSION

For the assessment of the feasibility of fs-LI-TOFMS for 3D imaging, the crater array and the morphology of the crater were investigated. Figure 2a shows the 30 × 30 spot array after 35 consecutive ablations on the self-prepared disc, which covers an area of 1.5 × 1.5 mm^2. A uniform pattern of equally distributed ablation craters can be observed. Figure 2b displays the morphology of the sectional craters from Figure 2a. It exhibits a series of craters with a diameter of approximately 50 μm and a relatively steep crater wall. Furthermore, the high quality and homogeneity ablation without thermal effect is presented. Given these, it is conceivable to perform 3D sampling by femtosecond laser ablation.

Because high irradiance fs-LI-TOFMS has little matrix effect and elemental fractionation, which results in more uniform relative sensitivities for most elements,[25] the elemental concentration can be acquired by a quantitation method without standards for calibration. The formula for the calculation is as follows:[31]

$$w_j = \sum_i A_{ij}M_{ij} / \sum_j \sum_i A_{ij}M_{ij}$$

where w_j represents the concentration of element j, while A_{ij} and M_{ij} define the peak area and the molar mass of isotope i of element j, respectively. This quantitation can be regarded as a 100%-mass-normalization approach; thus, the signal fluctuation of diverse craters, as well as different layers within the same crater, can be neglected.

To validate the 3D imaging ability of fs-LI-TOFMS, a self-prepared disc with four mixed powders of Cr, Fe, Ni, and Cu was subjected to fs-laser drilling at 30 × 30 spots, followed by TOFMS measurement for 200 shots per crater. The 3D distributions of these four elements can be seen in Figure 3a–d. Because of inhomogeneity in the mixture of the four powders and the diverse particle diameters even for the same metal, the elemental distribution characteristics vary with the particles. The particles with a diameter less than the drilling depth (140 μm) can be distinctly observed with a complete shape within the analytical volume. Moreover, irregular particle shapes can also be found in Figure 3, which is in agreement with the actual powders. Figure 3e is the combination of Figure 3a–d, which clearly shows the distribution of 4 types of metal particles in the cuboid section. This study reveals that the elemental distribution can be investigated via fs-LI-TOFMS not only laterally along the surface but also in the depth direction, even though it took approximately 5 h for the ablation and data acquisition.

DOI: 10.1021/acs.analchem.6b03540
Anal. Chem. 2017, 89, 565–570

The Nantan meteorite was investigated using the fs-LI-TOFMS system. The spectrum aggregating all the imaging data is shown in Figure 4, which indicates the meteorite contains Fe, Li, C, Na, Mg, Al, Si, P, S, K, Ca, Ti, V, Cr, Mn, Co, Ni, and Cu. The major, minor, and trace elemental compositions with well-matched isotope ratios are shown in the spectrum without significant interference.

A photograph of the Nantan iron meteorite with a highlighted imaging area and the 3D distributions of all elements are shown in Figure 5. The concentration of Fe (Figure 5b) within the whole imaged volume is high except for three small sections, which is in accordance with the fact that kamacite is the predominant mineral in iron meteorite.[4] Highly siderophile (iron-loving) elements (Co and Ni) have a similar distribution pattern (Figure 5c,d), which results from their almost identical condensation temperature and diffusion rate in Fe melt.[5,36] Primarily in the form of silicate inclusion, Si (Figure 5e) was predominantly located in the relatively low content zones of Fe, as their melts are immiscible and the density of the silicate melt is much lower.[4] Figure 5f–h shows very similar 3D distributions of Mg, Al, and K. Their crystallization might be in the form of mineral yagiite (a K–Mg–Al silicate).[37,38] Element Ca (Figure 5i) shows a very low content within the meteorite except for a small section on the surface (coordinates: x = 900 μm, y = 950 μm) which could be the high-Ca pyroxene as there Si has the highest concentration. Its formation likely involved local crystallization from a partial melting and melt migration.[37,39] Figure 5l reveals the overall concentration of Na in the upper section of the meteorite tends to be greater than that in the lower section. This might attribute to either the initial cooling taking place from the surface or surface contamination from the earth.[40] The chalcophile (S-loving) elements, Cu, Cr, V, and Mn, are generally partitioned into sulfide, which can be seen from Figure 5m–q. The other two nonmetal elements P (Figure 5r) and C (Figure 5s) have similar distributions to that of S, which could be attributed to rapid cooling leading to P- or C-rich melt enclosed in crystallizing sulfide.[3,41]

Two possible explanations could be assigned to the distinct 3D distributions of siderophile, lithophile, and chalcophile elements. On one hand, the content of S in the residual melt would increase, due to it being excluded from the process of crystallizing Fe metal. Siderophile elements were partitioned strongly into the Fe metal, while chalcophile elements had the opposite behavior.[42,43] On the other hand, silicon was reported to have little effect on the partitioning behaviors of all detected siderophile and chalcophile elements.[43,44] Thus, these three types of elements would be separated spatially.

CONCLUSION

A three-dimensional imaging mass spectrometry technique using fs-LI-TOFMS was applied for investigating the spatial distribution of elements in the Nantan meteorite with a spatial resolution in micrometers. The method is capable of semiquantitative analysis without standards for calibration. It is able to reach a detection limit of 10^{-6} g/g and a dynamic range of 6 orders of magnitude. The semiquantitative 3D imaging of 18 elements, including 4 nonmetal elements were exhibited. Different spatial patterns for various types of elements in the meteorite reveal its preliminary composition, fractionation, and thermal history, as well as its surrounding physical–chemical environment during formation and evolution.

AUTHOR INFORMATION

Corresponding Author

*E-mail: weihang@xmu.edu.cn.

ORCID

Wei Hang: 0000-0002-9145-3181

Notes

The authors declare no competing financial interest.

ACKNOWLEDGMENTS

We gratefully acknowledge the financial support from the Natural Science Foundation of China Financial (21427813). This work is also supported by the Program for Changjiang Scholars and the Innovative Research Team in University (IRT13036) and the Foundation for Innovative Research Groups of the National Natural Science Foundation of China (21521004).

REFERENCES

(1) Davis, A. M. *Meteorites, comets, and planets*; Elsevier: Oxford UK, 2005.

(2) Rudraswami, N.; Prasad, M. S.; Babu, E.; Kumar, T. V. *Geochim. Cosmochim. Acta* **2014**, *145*, 139–158.

(3) Goldstein, J.; Scott, E.; Chabot, N. *Chem. Erde* **2009**, *69*, 293–325.

(4) Wasson, J.; Kallemeyn, G. *Geochim. Cosmochim. Acta* **2002**, *66*, 2445–2473.

(5) Lodders, K. *Astrophys. J.* **2003**, *591*, 1220–1247.

(6) Petaev, M. I.; Wood, J. A. *Meteorit. Planet. Sci.* **1998**, *33*, 1123–1137.

(7) Pisonero, J.; Bordel, N.; Smentkowski, V. S. *J. Anal. At. Spectrom.* **2013**, *28*, 970–972.

(8) Tomkins, A. G.; Mare, E. R.; Raveggi, M. *Geochim. Cosmochim. Acta* **2013**, *117*, 80–98.

(9) Festa, G.; Cippo, E. P.; Di Martino, D.; Cattaneo, R.; Senesi, R.; Andreani, C.; Schooneveld, E.; Kockelmann, W.; Rhodes, N.; Scherillo, A.; et al. *J. Anal. At. Spectrom.* **2015**, *30*, 745–750.

(10) Garrevoet, J.; Vekemans, B.; Tack, P.; De Samber, B.; Schmitz, S.; Brenker, F. E.; Falkenberg, G.; Vincze, L. *Anal. Chem.* **2014**, *86*, 11826–11832.

(11) Vincze, L.; Vekemans, B.; Brenker, F. E.; Falkenberg, G.; Rickers, K.; Somogyi, A.; Kersten, M.; Adams, F. *Anal. Chem.* **2004**, *76*, 6786–6791.

(12) Silversmit, G.; Vekemans, B.; Appel, K.; Schmitz, S.; Schoonjans, T.; Brenker, F. E.; Kaminsky, F.; Vincze, L. *Anal. Chem.* **2011**, *83*, 6294–6299.

(13) Hou, H.; Cheng, L.; Richardson, T.; Chen, G.; Doeff, M.; Zheng, R.; Russo, R.; Zorba, V. *J. Anal. At. Spectrom.* **2015**, *30*, 2295–2302.

(14) Lucena, P.; Laserna, J. J. *Spectrochim. Acta, Part B* **2001**, *56*, 177–185.

(15) Alvarez, C.; Pisonero, J.; Bordel, N. *Spectrochim. Acta, Part B* **2014**, *100*, 123–128.

(16) Fortes, F. J.; Moros, J.; Lucena, P.; Cabalín, L. M.; Laserna, J. J. *Anal. Chem.* **2013**, *85*, 640–669.

(17) Kuznetsov, I.; Filevich, J.; Dong, F.; Woolston, M.; Chao, W.; Anderson, E. H.; Bernstein, E. R.; Crick, D. C.; Rocca, J. J.; Menoni, C. S. *Nat. Commun.* **2015**, *6*, 6944.

(18) Wirtz, T.; Fleming, Y.; Gysin, U.; Glatzel, T.; Wegmann, U.; Meyer, E.; Maier, U.; Rychen, J. *Surf. Interface Anal.* **2013**, *45*, 513–516.

(19) Chirinos, J. R.; Oropeza, D. D.; Gonzalez, J. J.; Hou, H.; Morey, M.; Zorba, V.; Russo, R. E. *J. Anal. At. Spectrom.* **2014**, *29*, 1292–1298.

(20) van Elteren, J. T.; Izmer, A.; Šala, M.; Orsega, E. F.; Šelih, V. S.; Panighello, S.; Vanhaecke, F. *J. Anal. At. Spectrom.* **2013**, *28*, 994–1004.

DOI: 10.1021/acs.analchem.6b03540
Anal. Chem. 2017, 89, 565–570

(21) Peng, S.; Hu, Q.; Ewing, R. P.; Liu, C.; Zachara, J. M. *Environ. Sci. Technol.* **2012**, *46*, 2025−2032.
(22) Burger, M.; Gundlach-Graham, A. W.; Allner, S.; Schwarz, G.; Wang, H. A.; Gyr, L.; Burgener, S.; Hattendorf, B.; Grolimund, D.; Günther, D. *Anal. Chem.* **2015**, *87*, 8259−8267.
(23) Gutierrez-Gonzalez, A.; Gonzalez-Gago, C.; Pisonero, J.; Tibbetts, N.; Menendez, A.; Velez, M.; Bordel, N. *J. Anal. At. Spectrom.* **2015**, *30*, 191−197.
(24) He, M. H.; Li, B.; Yu, S. Y.; Zhang, B. C.; Liu, Z. H.; Hang, W.; Huang, B. L. *J. Anal. At. Spectrom.* **2013**, *28*, 499−504.
(25) Zhang, B. C.; He, M. H.; Hang, W.; Huang, B. L. *Anal. Chem.* **2013**, *85*, 4507−4511.
(26) Russo, R. E.; Mao, X.; Gonzalez, J. J.; Mao, S. S. *J. Anal. At. Spectrom.* **2002**, *17*, 1072−1075.
(27) Gonzalez, J.; Dundas, S. H.; Liu, C. Y.; Mao, X.; Russo, R. E. *J. Anal. At. Spectrom.* **2006**, *21*, 778−784.
(28) Li, L. F.; Zhang, B. C.; Huang, R. F.; Hang, W.; He, J.; Huang, B. L. *Anal. Chem.* **2010**, *82*, 1949−1953.
(29) Huang, R. F.; Yu, Q.; Li, L.; Lin, Y.; Hang, W.; He, J.; Huang, B. *Mass Spectrom. Rev.* **2011**, *30*, 1256−1268.
(30) He, M. H.; Xiao, Y. F.; Zhang, S. D.; Liu, R.; Hang, W.; Huang, B. L. *Appl. Surf. Sci.* **2015**, *351*, 624−634.
(31) Huang, R. F.; Zhang, B. C.; Zou, D. X.; Hang, W.; He, J.; Huang, B. L. *Anal. Chem.* **2011**, *83*, 1102−1107.
(32) Grimaudo, V.; Moreno-Garcia, P.; Riedo, A.; Neuland, M. B.; Tulej, M.; Broekmann, P.; Wurz, P. *Anal. Chem.* **2015**, *87*, 2037−2041.
(33) Cui, Y.; Moore, J. F.; Milasinovic, S.; Liu, Y.; Gordon, R. J.; Hanley, L. *Rev. Sci. Instrum.* **2012**, *83*, 093702.
(34) Onuma, N.; Notsu, K.; Nishida, N.; Wakita, H.; Takeda, H.; Nagasawa, H.; Ouyang, Z. Y.; Wang, D. D. *Diqiu Huaxue* **1979**, 52−60.
(35) Kim, M. K.; Takao, T.; Oki, Y.; Maeda, M. *Jpn. J. Appl. Phys., Part 1* **2000**, *39*, 6277−6280.
(36) Righter, K.; Campbell, A.; Humayun, M. *Geochim. Cosmochim. Acta* **2005**, *69*, 3145−3158.
(37) Ruzicka, A. *Chem. Erde* **2014**, *74*, 3−48.
(38) Ruzicka, A.; Hutson, M.; Floss, C. *Meteorit. Planet. Sci.* **2006**, *41*, 1797−1831.
(39) Ruzicka, A.; Hutson, M. *Geochim. Cosmochim. Acta* **2010**, *74*, 394−433.
(40) Chen, M.; Xie, X. D. *Eur. J. Mineral.* **1996**, *8*, 325−333.
(41) Luecke, W.; Kontny, A.; Kramar, U. *Meteorit. Planet. Sci.* **2014**, *49*, 750−771.
(42) Chabot, N. L.; Saslow, S. A.; McDONOUGH, W. F.; Jones, J. H. *Meteorit. Planet. Sci.* **2009**, *44*, 505−519.
(43) Chabot, N. L.; Agee, C. B. *Geochim. Cosmochim. Acta* **2003**, *67*, 2077−2091.
(44) Chabot, N. L.; Safko, T. M.; McDONOUGH, W. F. *Meteorit. Planet. Sci.* **2010**, *45*, 1243−1257.

DOI: 10.1021/acs.analchem.6b03540
Anal. Chem. 2017, 89, 565−570